Int. J. Appl. Math. Comput. Sci., 2023, Vol. 33, No. 2, 207–218
DOI: 10.34768/amcs-2023-0016

A DYNAMIC SUBMERGING MOTION MODEL OF THE HYBRID–PROPELLED UNMANNED UNDERWATER VEHICLE: SIMULATION AND EXPERIMENTAL VERIFICATION

TOMASZ TALARCZYK [a]

[a] Faculty of Mechanical Engineering
Cracow University of Technology
Al. Jana Pawła II 37, 31-864 Cracow, Poland
e-mail: tomasz.talarczyk@pk.edu.pl

Hybrid propulsion in underwater vehicles is the new idea of combining conventional propulsion systems such as screw propellers with other kinds of propulsion like oscillating biomimetic fins, glider wings or jet thrusters. Each of these propulsion systems has its own benefits and drawbacks, and the goal is to have them complement each other in certain conditions. This paper covers the topic of a dynamic model of the pitch and heave motion of the HUUV (hybrid unmanned underwater vehicle) using screw propellers and biomimetic lateral fins. Firstly, the simulation model of the vehicle performing depth and pitch change is presented. Secondly, the vehicle's hydrodynamic coefficients obtained from CFD simulations are discussed. Thirdly, the results of the HUUV experimental studies in a swimming pool are presented. Lastly, simulation results are compared with those of the experiment to verify the correctness of the model. The vehicle's motion in the swimming pool during the experiments was recorded using a submerged camcorder and then analysed using the Tracker software.

Keywords: autonomous underwater vehicles, hybrid propulsion system, biomimetic underwater vehicles, dynamic diving, diving model.

1. Introduction

Combining screw propellers and oscillating fins in a single underwater vehicle offers the ability to utilize advantages of biomimetic fish-like mobile robots (Morawski *et al.*, 2014) with their silent undulating propulsion (Malec and Morawski, 2014; Piskur *et al.*, 2021). Such a combination comes at a cost of limitation of the vehicle's resemblance to a real aquatic vehicle. In consequence, a torpedo-shaped vehicle with biomimetic fins is created (Morawski *et al.*, 2018, 2021). The dynamics of underwater vehicles have been studied intensively in the last years. The most popular approach to deriving the model of motion was proposed by Fossen (2011) and most researchers use this model to simulate vehicles' motion. Assumptions such as torpedo-like shape, three planes of symmetry and a small distance between the centre of buoyancy and that of gravity were made in order to maximally simplify the equations of motion.

In work of Kim and Choi (2004), from a 6DOF model, two models in vertical (xz) and horizontal (xy) planes were extracted. Assumptions such as three planes of symmetry and a torpedo-shaped vehicle were made. The vehicle was propelled by two thrusters placed at the stern and stern planes to control the pitch movement. Ha *et al.* (2008) used the same model to simulate different control strategies. A similar approach was presented by Steenson *et al.* (2012), Zhou *et al.* (2015), Huy *et al.* (2016), Chae (2021) or Desai and Manjarekar (2021), with a difference in the propulsion system. The vehicles were equipped with one screw propeller at the stern and stern planes to control the pitch and yaw movements.

In the work of Shrivastava *et al.* (2021) a 6-DOF model was presented and simulated with a torpedo-shape vehicle. The vehicle was equipped with four thrusters: two on starboard and portboard to control the horizontal movement and two at the stern and bow to control the vertical movement. In the work of Zeng *et al.* (2017) the vehicle with a mast on top was presented. The propulsion system consists of one screw propeller at the stern and control planes in the horizontal and vertical planes. A vehicle with a non-torpedo shape propelled

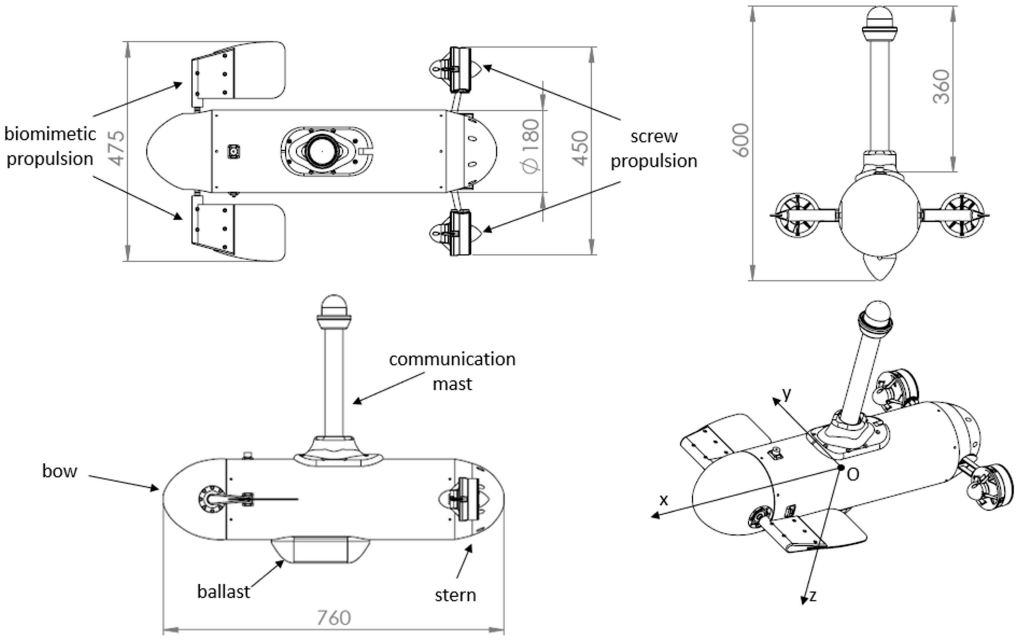

Fig. 1. View and dimensions of the HUUV.

by thrusters in the horizontal and vertical planes was presented by Szymak *et al.* (2021) and simulated in 6-DOF. In the works of Horak *et al.* (2020) as well as Maalouf *et al.* (2015), Fossen's mathematical model was used to simulate the motion of a remote operated vehicle (ROV) with a complex shape geometry. In the work of Liu *et al.* (2023), a model of a complex-shape underwater towed vehicle was presented with no propulsion system. The vehicle was equipped with control planes in the horizontal and vertical planes. Another approach to modelling the motion of torpedo-shaped vehicles was proposed by Ladyżyńska-Kozdraś (2012). The equations of movement were derived using analytical mechanic Maggi equations. This approach was later verified by Ładyżyńska-Kozdraś (2014b; 2014a).

In some cases the aforementioned assumptions cannot be accepted because this will provide inaccurate simulation data. In the works of Petrich *et al.* (2007) as well as Petrich and Stilwell (2010) another approach was proposed. The model was expanded and the velocity vector (which is not in coincidence with the longitudinal axis of the vehicle) equation was extracted. This means that the depth motion does not only depend on the pitch angle of a vehicle but also on the angle of the attack between the vehicle's longitudinal axis and the velocity vector. This concept of the velocity vector equation has not been intensively developed in the literature because of the simplicity of Fossen's equations.

In this paper, a simulation model of diving motion of a hybrid unmanned underwater vehicle (HUUV) is derived and verified with experimental data. The HUUV is equipped with a communication mast. This caused the high asymmetry in the horizontal plane and does not allow model simplification as presented in the literature, so the model with a velocity vector equation is used. To simulate diving motion, parameter identification is done. Hydrodynamic coefficients are estimated using CFD simulations according to Sakaki and Kerdabadi (2020). Inertia coefficients are calculated following Severholt (2017).

The paper is organized as follows. In Section 2, the depth change subsystem of the HUUV is presented. In Section 3, the mathematical model of diving motion is derived and presented in the Scilab Xcos software. In Section 4, the hydrodynamic and inertia coefficient of the HUUV is investigated. In Section 5, experimental tests conducted with the vehicle are described. In Section 6, simulation end experimental data comparison is discussed.

2. Depth control subsystem

The HUUV (Fig. 1) was designed and constructed to combine advantages of different types of propulsion, screw and biomimetic in one vehicle. The first one, placed at the stern, is able to generate a high amount of thrust force, which allows the vehicle to move fast with a high dynamic, but it is loud and not very energy efficient. The second one (biomimetic), placed at the bow, uses two oscillating lateral fins to generate the thrust force and a specially designed mechanism which allows the fins to change their angles of attack.

The HUUV's combined propulsion system allows moving the vehicle in two ways. One is using two screw propellers and changing the depth and the pitch angle by changing the angle of attack of lateral fins. The course change is done by generating a different thrust for each propeller. The other way of motion is using only oscillating lateral fins and changing the vehicle's depth by changing neutral points of oscillations of both fins simultaneously. In this case the course of the vehicle is changed by different oscillation parameters for the left and the right fin. The HUUV has only one main plane of the symmetry (x-z). The vehicle is not symmetrical in the x-y plane because of the communication mast placed on top of the vehicle and the ballast placed at the bottom. In this paper the dynamic depth control using screw propellers and lateral fins is presented. The change in the depth is done by changing the deflection angle of both the lateral fins simultaneously. The mass, principal moments of inertia and the centre of gravity parameters of the vehicle presented in Table 1 were obtained using the CAD model of the vehicle by the Solidworks® software.

3. Simulation model

To simulate the diving motion of the HUUV, the model of the vehicle based on the results of Petrich *et al.* (2007) was used. One of the most important aspects of the HUUV's diving motion is to maintain a possibly small pitch angle in order for the optical communication system, with a camcorder placed on top of the vehicle's mast, to work properly. This camcorder placement, along with a small pitch angle for the moving vehicle, allows implementing in the control software simple vision processing algorithms. To achieve small pitch angles, a massive ballast was attached to the bottom of the vehicle. This made the centre of mass go down and the vehicle gain the restoring moment, which provides the stability of movement and the required small pitch angle during diving, but caused the angle attack of the vehicle speed and the pitch angle to differ. This means that the vehicle speed vector does not coincide with the x axis. To properly simulate the diving motion of the HUUV, the model provided by Petrich *et al.* (2007) was used. The model uses simplified Kirchhoff equations of motion, cf. (1). The main parameters of the model are presented in Fig. 2. A global coordination system is denoted as (XYZ) with the Y axis pointing out from the picture. A local (body) coordination system is denoted as (xyz). A negative pitch angle means the vehicle bow is directed down. Specifically, we have

$$M\dot{x} = R(x) + F(x,u) \tag{1}$$

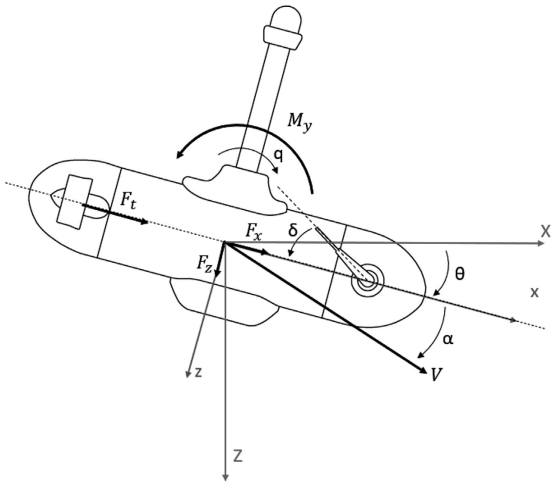

Fig. 2. Pitch axis model for the HUUV traveling at speed V with angle of attack α.

Table 1. Mass, moments of inertia and the centre of gravity.

Parameter	Value	Units	Parameter	Value	Units
m	18.93	kg	I_{zz}	0.68	kg · m^2
I_{xx}	0.18	kg· m^2	x_{cg}	0.01	m
I_{yy}	0.63	kg· m^2	z_{cg}	0.03	m

with the parameters

$$M = \begin{bmatrix} m_x & 0 & mz_{cg} \\ 0 & m_z & -mx_{cg} \\ mz_{cg} & -mx_{cg} & J_y \end{bmatrix},$$

$$\dot{x} = \begin{bmatrix} \dot{u} \\ \dot{w} \\ \dot{q} \end{bmatrix}, \quad F(x,u) = \begin{bmatrix} F_x\,(V,\alpha,\theta,\delta) \\ F_z\,(V,\alpha,\theta,\delta) \\ M_y\,(V,\alpha,\theta,\delta) \end{bmatrix},$$

$$R(x) = \begin{bmatrix} -m_z wq \; - mx_{cg}q^2 \\ m_x uq + mz_{cg}q^2 \\ (m_z - m_x)\,uw \; - mq(ux_{cg} + wz_{cg}) \end{bmatrix},$$

where m_x, m_z denote the dry masses of the vehicle plus added masses in the x and z directions, respectively, u, w, q mean the surge, heave and pitch velocities of the vehicle, respectively, J_y is the moment of inertia around the y axis including the moment of inertia of the added mass, x_{cg}, y_{cg}, z_{cg} are the coordinates of the vehicle's centre of gravity in the local reference frame, α, θ, δ stand for the angle of attack, the pitch angle, the fin deflection angle, respectively, F_x, F_z, M_y the are external forces and the torque.

External forces F_x, F_z and torque M_y depend on weight force F_w, buoyancy force F_b, thrust force F_t, hydrodynamic forces drag F_D, lift F_L and torque M_q.

The equations representing these loads are as follows, while the drag force generated by fins has been omitted:

$$\begin{aligned} F_x(V,\alpha,\theta,\delta) &= \cos\alpha\, F_D(V,\alpha,\delta) \\ &\quad - \sin\alpha\, F_L(V,\alpha,\delta) \\ &\quad - (F_w - F_b)\sin\theta + F_t, \qquad (2) \\ F_z(V,\alpha,\theta,\delta) &= \sin\alpha\, F_D(V,\alpha,\delta) \\ &\quad - \cos\alpha\, F_L(V,\alpha,\delta) \\ &\quad - (F_w - F_b)\cos\theta, \qquad (3) \\ M_y(V,\alpha,q,\theta,\delta) &= M_q(V,\alpha,q,\delta) \\ &\quad - (x_{cg}\cos\theta + z_{cg}\sin\theta)F_w, \qquad (4) \\ F_D(V,\alpha,\delta) &= \frac{1}{2}\rho V^2 A_b C_D\,, \qquad (5) \\ F_L(V,\alpha,\delta) &= \frac{1}{2}\rho V^2(A_b C_{L\alpha}\,\alpha + A_f C_{L\delta}\,\delta), \qquad (6) \\ M_q(V,\alpha,q,\delta) &= \frac{1}{2}\rho V^2[A_b L\,(C_{m\alpha}\alpha + C_{mq}q) \\ &\quad +\ A_f x_f C_{L\delta}\,\delta]. \qquad (7) \end{aligned}$$

The model (1)–(7) defines the surge (u), heave (w) and pitch (q) velocities of the vehicle in the moving reference frame whose origin is located in the centre of buoyancy of the vehicle. The vector of velocity of the HUUV (V) does not coincide with the x axis, so the model (1) is extended with additional components in which the velocity vector was decomposed into components u and w according to

$$u = V\cos\alpha, \quad w = V\sin\alpha. \qquad (8)$$

This means that the velocity does not coincide with the x axis and there is an angle of attack α. The time derivative of (8) is

$$\begin{bmatrix}\dot u\\ \dot w\end{bmatrix} = \begin{bmatrix}\cos\alpha & -V\sin\alpha\\ \sin\alpha & V\cos\alpha\end{bmatrix}\begin{bmatrix}\dot V\\ \dot\alpha\end{bmatrix}. \qquad (9)$$

Using (1)–(9), the vehicle's control model based on the state vector and input

$$x = \begin{bmatrix}V\\ \alpha\\ q\\ \theta\end{bmatrix}, \qquad i = \delta \qquad (10)$$

was derived in the following form:

$$MT(x)\,\dot x = R(x) + F(x,i), \qquad (11)$$

where

$$M = \begin{bmatrix} m_x & 0 & mz_{cg} & 0\\ 0 & m_z & -mx_{cg} & 0\\ mz_{cg} & 0 & J_y & 0\\ 0 & 0 & 0 & 1\end{bmatrix},$$

$$T(x) = \begin{bmatrix}\cos\alpha & -V\sin\alpha & 0 & 0\\ \sin\alpha & V\cos\alpha & 0 & 0\\ 0 & 0 & 1 & 0\\ 0 & 0 & 0 & 1\end{bmatrix},$$

$$F(x,i) = \begin{bmatrix}F_x(x,i)\\ F_z(x,i)\\ M_y(x,i)\\ 0\end{bmatrix},$$

$$R(x) = \begin{bmatrix} -m_z qV\sin\alpha - mx_{cg}q^2\\ m_x qV\cos\alpha + mz_{cg}q^2\\ [(m_z - m_x)V^2\cos\alpha\sin\alpha\\ -mqV(\cos\alpha x_{cg} + \sin\alpha z_{cg})]\\ q\end{bmatrix}.$$

In accordance with the linearization from the Petrich *et al.* (2007), the final model of vehicle diving is

$$\begin{bmatrix}\dot V\\ \dot\alpha\\ \dot q\\ \dot\theta\end{bmatrix} = \begin{bmatrix} a_{11} & 0 & 0 & 0\\ 0 & a_{22} & a_{23} & 0\\ 0 & a_{32} & a_{33} & a_{34}\\ 0 & 0 & 1 & 0\end{bmatrix}\begin{bmatrix}V\\ \alpha\\ q\\ \theta\end{bmatrix} + \begin{bmatrix}0\\ b_{21}\\ b_{31}\\ 0\end{bmatrix}\delta, \qquad (12)$$

where the system parameters are as follows:

$$\begin{aligned} a_{11} &= \frac{1}{m_x}\rho\, V A_b C_{D\alpha},\\ a_{33} &= \frac{1}{2J_y}\rho\, V^2 A_b L C_{mq},\\ a_{22} &= \frac{1}{2m_z}\rho\, V A_b\,(C_{D\alpha} + C_{L\alpha})\,,\\ a_{34} &= -\frac{1}{J_y}z_{cg}F_w,\\ a_{23} &= \frac{m_x}{m_z},\\ a_{32} &= \frac{1}{J_y}\left[(m_z - m_x)\,V^2 + \frac{1}{2}\rho V^2 A_b L C_{m\alpha}\right],\\ b_{21} &= \frac{1}{2m_z}\rho\, V A_f C_{L\delta},\\ b_{31} &= \frac{1}{2J_y}\rho\, V^2 A_f x_f C_{L\delta}. \end{aligned}$$

Here A_b is the vertical cross-section area of the vehicle (in the x axis), A_f is the reference surface area of fins, x_f is the distance from the center of buoyancy to the location of forces acting on the fins, L is the reference length of the vehicle, $C_{D\alpha}, C_{L\alpha}, C_{m\alpha}, C_{mq}, C_{L\delta}$ are the drag, lift, body's restoring moment, viscous damping and fins lift coefficients, respectively.

The state vector consists of four main elements: the speed of the vehicle (V), the angle of attack of the velocity vector (α), the speed of the vehicle rotation (q) and the pitch angle of the vehicle (θ). To determine the diving motion according to Fig. 2, the velocity vector is first projected onto the vehicle coordinate system x, y, z using the angle of attack α, and then onto the global coordinate system X, Y, Z using θ. Thus the heave is

$$\dot{Z} = V\left[-\cos\alpha\sin\theta + \sin\alpha\cos\theta\right]. \tag{13}$$

The simulation model presented in Appendix was implemented in the SciLab Xcos software. The output of the simulation is the speed of the vehicle V, angle θ and depth Z. The input is the thrust force and the angle of fin deflection δ.

4. Hydrodynamic and inertial coefficients

The model presented in Section 2 uses hydrodynamic coefficients and inertial coefficients (added masses). Hydrostatic coefficients, due to the assumption that the vehicle is neutrally buoyant, were not designated and the effect of hydrostatic force is not included in the model. Hydrodynamic coefficients $C_{D\alpha},\ C_{L\alpha},\ C_{m\alpha}, C_{mq}, C_{L\delta}$ were obtained using CFD simulation in the SimScale software. Inertial coefficients were determined analytically. To calculate hydrodynamic coefficients, the method presented by (Sakaki and Kerdabadi, 2020) was used. To obtain all the five coefficients, three different types of CFD simulations were performed.

4.1. Hydrodynamic coefficients depending on the angle of attack α. The first type refers to $C_{D\alpha},\ C_{L\alpha},\ C_{m\alpha}$. Simulations were performed with the computational domain and mesh presented in Figs. 3 and 4, with the parameters listed in Table 2.

In the static pitch test, the forces and torques with a different angle of attack α of the vehicle were measured. The obtained coefficients are presented in Figs. 5–7. Based on the results of CFD analysis, the hydrodynamic coefficients values were numerically interpolated using the least-squares method. The obtained formulae are presented in Table 3.

4.2. Hydrodynamic coefficients depending on rotational velocity. The second type of CFD simulations refers to C_{mq} hydrodynamic coefficient which describes the damping effect of vehicle rotation. Inside the computational domain presented in Figs. 8 and 9, a cylindrical region was defined with more dense mesh. The SimScale software allows simulating the rotating domain called the moving reference frame (MRF) with a defined rotational velocity. In this simulation, performed with parameters presented in Table 4, the linear velocity of the fluid inside the computational domain is close to zero and the forces are derived from the rotation of the fluid around a stationary vehicle. MRF simulations allowed obtaining a hydrodynamic coefficient depending on rotation velocity q. The rotation damping coefficient is $C_{mq} = -4.4784q$.

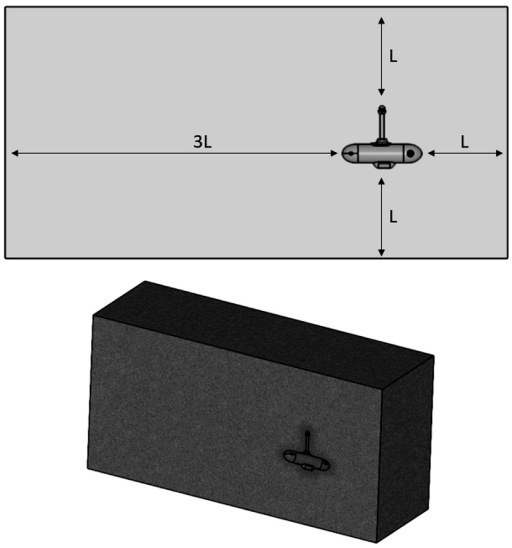

Fig. 3. Computational domain around the HUUV.

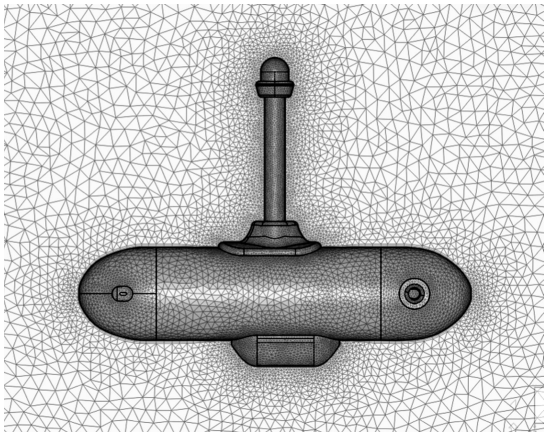

Fig. 4. Mesh generated in the computational domain.

Table 2. Parameters of CFD simulation.

Number of cells	1.5 M
Turbulence model	k-Omega SST
Time dependency	Steady-state
Algorithm	SIMPLE

Table 3. Formulae for calculating hydrodynamic coefficients depending on the angle of attack α.

Drag C_{D_α}	$-4.3581\alpha^2 - 0.0276\alpha - 0.5213$
Lift C_{L_α}	$3.7385\alpha - 0.0078$
Moment C_{M_α}	$-1.0047\alpha - 0.066$

Table 4. Parameters of MRF CFD simulations.

Number of cells	5.5M
Turbulence model	k-omega SST
Time dependency	Steady-state
Algorithm	SIMPLE

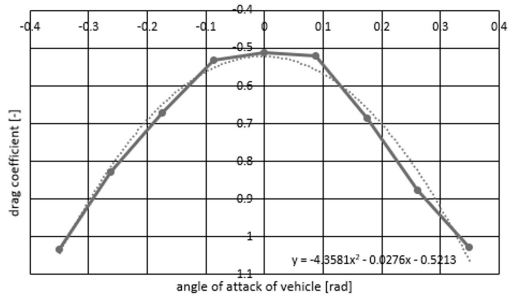

Fig. 5. Drag coefficient C_{D_α}.

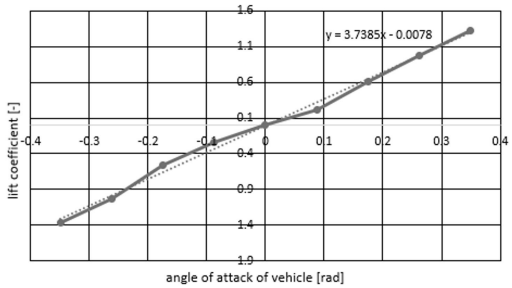

Fig. 6. Lift coefficient C_{L_α}.

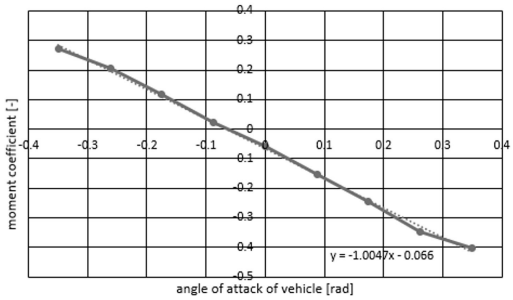

Fig. 7. Moment coefficient C_{M_α}.

Table 5. Parameters of a single fin CFD simulation.

Number of cells	4.7M
Turbulence model	k-omega SST
Time dependency	Steady-state
Algorithm	SIMPLE

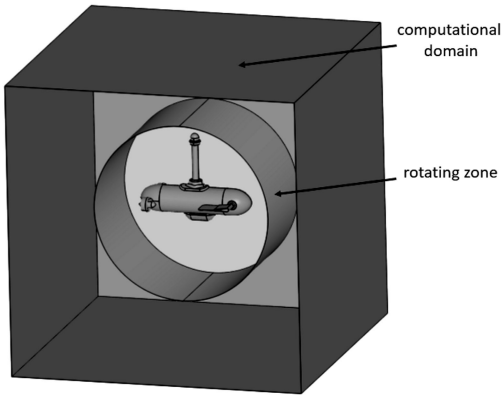

Fig. 8. Computational domain with a rotating zone around the HUUV.

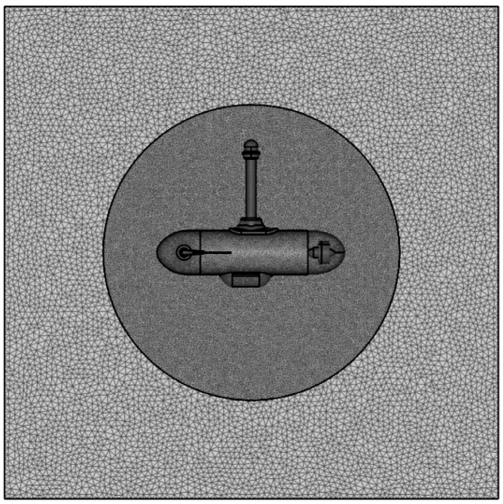

Fig. 9. Mesh generated around the HUUV.

4.3. Hydrodynamic coefficients generated by fins. The last type of simulation concerns the lift force, generated by fins at different deflection angles δ. An analysis of the fin drag force was presented by Piskur *et al.* (2020). Based on that, the lift force of the fin was obtained. The fin itself was simulated with the parameters presented in Table 5. The results of the simulations are shown in Fig. 10. Based on the simulations, the lift coefficient of a single fin depends on its deflection angle and is expressed as $C_{L\delta} = 0.0426\delta$.

4.4. Inertial (acceleration) coefficients. The simulation model requires three inertial coefficients: m_x, m_z, J_y. The first two refer to added masses of surrounding water in the x and z axes, respectively, and the third one refers to the added mass of water in the rotation movement around the vehicle's centre of buoyancy. These acceleration coefficients were calculated according to the empirical formulae of acceleration of a cylinder in water. The vehicle's shape was approximated with two cylinders representing the hull and mast. Added

masses were calculated using

$$m_x = m + m_{\dot{x}\text{hull}} + m_{x\text{mast}} = m + 0.1m_{\text{vehicle}} + \pi\rho {r_{\text{mast}}}^2 L_{\text{mast}}, \quad (14)$$

$$m_z = m + m_{\dot{z}\text{hull}} + m_{\dot{z}\text{mast}} = m + \pi\rho {r_{\text{hull}}}^2 L_{\text{hull}} + 0, \quad (15)$$

In Eqn. (15) the added mass of mast in the z direction is very small in comparison with the hull and is omitted:

$$J_y = I_y + J_{\dot{y}\text{hull}} + J_{\dot{y}\text{mast}} = I_y + \frac{1}{12}\pi\rho {r_{\text{hull}}}^2 {L_{\text{hull}}}^3 + \frac{1}{6}\pi\rho {r_{\text{mast}}}^2 (2L_{\text{mast}})^3, \quad (16)$$

where $r_{\text{mast}} = 0.02\,\text{m}$, $L_{\text{hull}} = 0.76\,\text{m}$, $r_{\text{hull}} = 0.09$ m, $m_{\text{vehicle}} = 18.5\text{kg}$, $L_{\text{mast}} = 0.35$ m.

5. Experimental tests

Two different tests were performed to examine the speed, depth and change in the pitch angle of the vehicle in motion. Both tests were conducted in still water in a 1.2 m deep swimming pool.

The first test was a complete one, in which the vehicle's diving motion was examined in a whole spectrum of speeds and deflection angles of fins. During experiments the vehicle was connected to the PC computer via a tether with neutral buoyancy and the buoyancy of the vehicle was slightly positive, so the top of the mast was 5 cm above the water surface when the vehicle was stopped. A series of tests were conducted for different powers of thrusters: 28, 40, 52, 64, 76, 88, 100% of maximal power. For each power level, a series of six runs were done with different angles of fin deflection: 15, 20, 25, 30, 35, 40°. Each run was repeated three times. The power range of thrusters from 0 to 28% and the fin angles from 0 to 15° were omitted due to the negligible effect on the vehicle's draft. The force generated by fins in those runs was so small that the vehicle did not begin to descend; on the contrary, it surfaced due to the resistance generated by the mast. One of the tests for 76% power of thrusters is presented in Figs. 11 and 12.

The second test consisted in combining data from two different sources: from sensors in the vehicle and obtained with the vehicle motion registered on video and then analysed in the Tracker software. Image analysis is a very popular solution in motion analysis of underwater robotic (Jurczyk *et al.*, 2020; Piskur, 2022). In order to perform motion analysis of the vehicle, the GoPro® Hero 6 camcorder was placed on a stand under the water surface. The vehicle moved across the field of view of the camcorder and subsequent tests were recorded. Then, the Tracker software was used to analyse the location of markers, placed on the side of the vehicle, in the

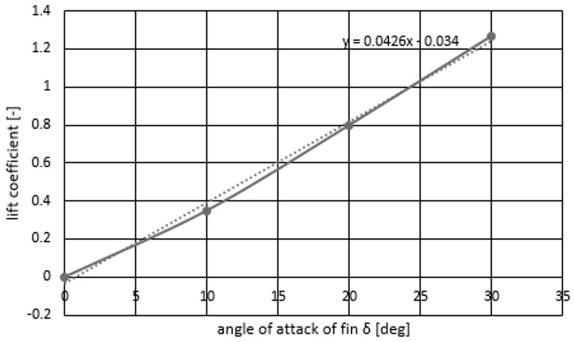

Fig. 10. Lift coefficient generated by a fin with different deflection angles δ.

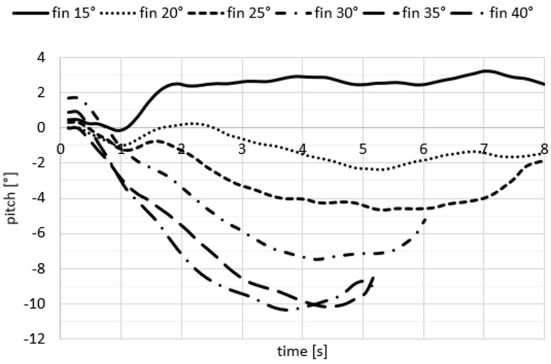

Fig. 11. Pitch angle change in time for thruster power of 76% with different deflection angles of fins.

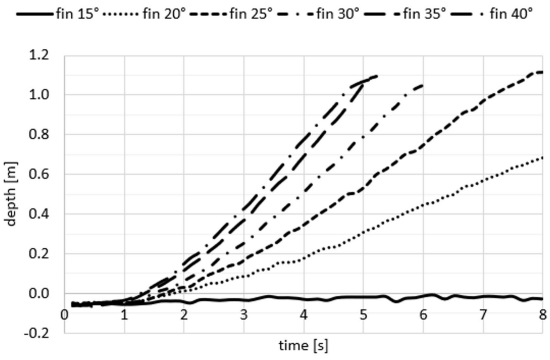

Fig. 12. Depth change in time for thruster power of 76% with different deflection angles of fins.

video frame. The system was calibrated based on the actual distance between those markers attached to the side of the vehicle. Having the position of markers in the coordinate system of a video frame and the calibrated distance between them, calculation of subsequent marker positions and velocities in the following frames as well as the theta angle of the vehicle was performed.

A single frame of video in the Tracker window is presented in Fig. 13. In this test, the vehicle was moving with 68% of thruster power and the fin deflection change is presented in Fig. 14. Sensors mounted inside the vehicle

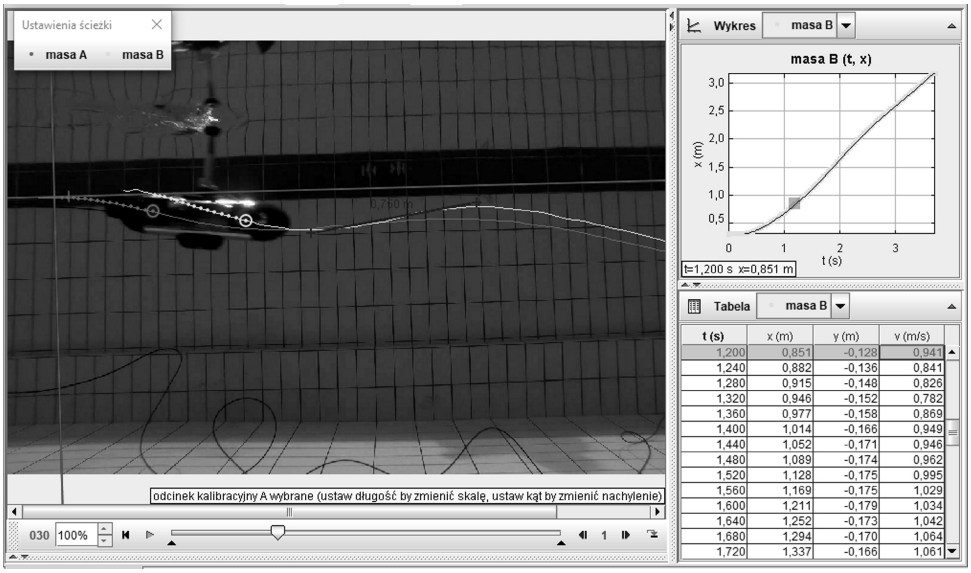

Fig. 13. Video analysis of diving motion of the HUUV in Tracker.

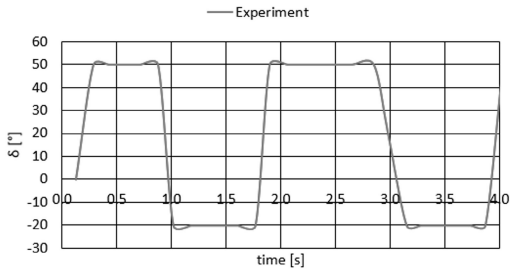

Fig. 14. Fin deflection angle for a diving test (input).

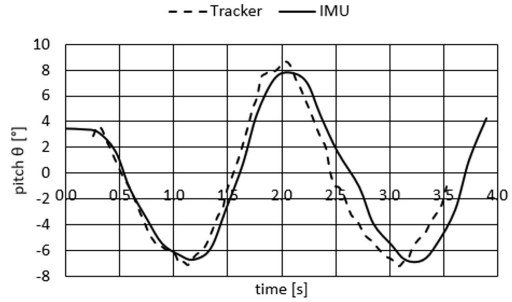

Fig. 15. Pitch angle change in experimental and tracker tests.

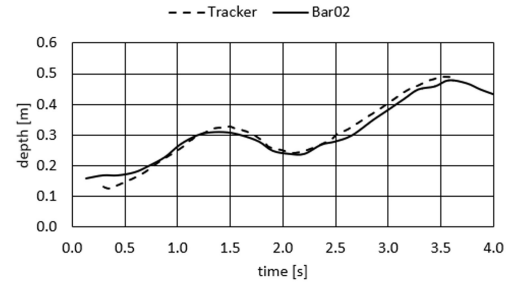

Fig. 16. Depth change in experimental and tracker tests.

provided the depth (Bluerobotis Bar02 pressure sensor) and pitch angle (VectorNav VN-100 Inertial Measurement Unit). Data obtained from the video analysis additionally provided the speed of the vehicle. The experimental results are presented in Figs. 15 and 16.

6. Simulation tests

Simulations of diving motion with the same input signals as in the experimental tests were performed and their results were compared with the first experimental data. The first comparison was made with results of the experimental test. Selected series with different speeds and fin deflection angles are presented in Figs. 17–19.

In Fig. 17(a) the first four seconds of motion are an unsteady phase in which the vehicle starts changing the pitch angle. In this stage, the experimental data show small oscillations that are not noticeable on the simulation run. In the experimental tests the vehicle started runs with slightly positive buoyancy (the depth in time $= 0$ is about 30 cm) so the small part of the mast (about 5 cm) was above the water surface. The model assumes neutral buoyancy so the curve obtained from the simulation immediately went down. The same situation is presented in Fig. 18(a). There are a couple of plausible reasons of this oscillations. Firstly, the model does not analyze the drag generated by the mast partially protruding from the water. Secondly, the thrust force generated by the propellers was simplified as a force in time, not as a rotational speed of the propeller, so the rotational speed is unknown. Despite the fact that during the experimental tests a small piece of the mast was above the water surface, in the initial phase of the movement, the vehicle did not emerge sufficiently to make the propellers

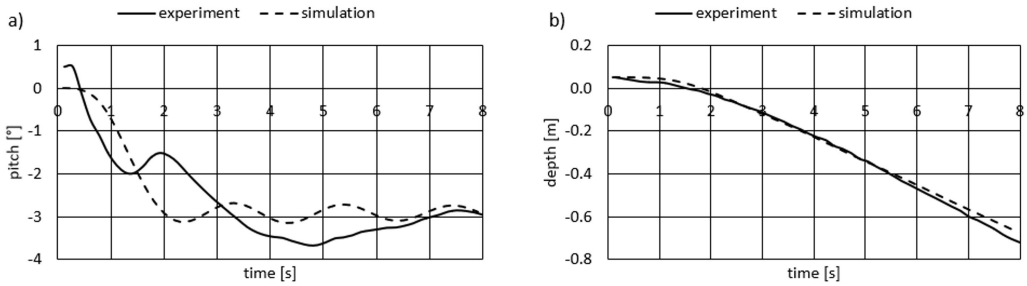

Fig. 17. Pitch angle (a) and depth (b) of the vehicle with fin angle $\delta = 30°$ and velocity $V = 0.65$ m/s.

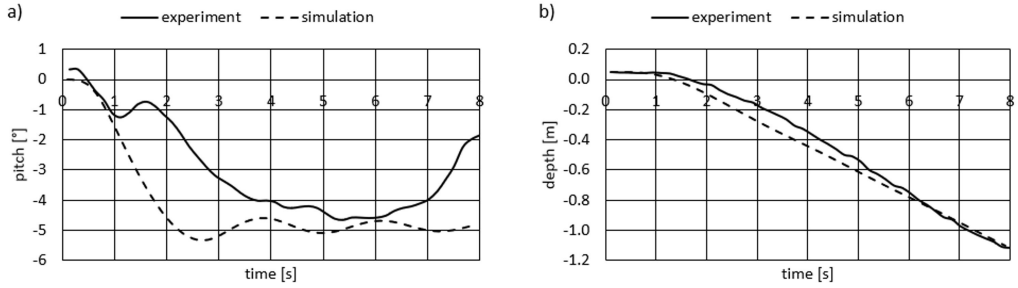

Fig. 18. Pitch angle (a) and depth (b) of the vehicle with fin angle $\delta = 25°$ and velocity $V = 1$ m/s.

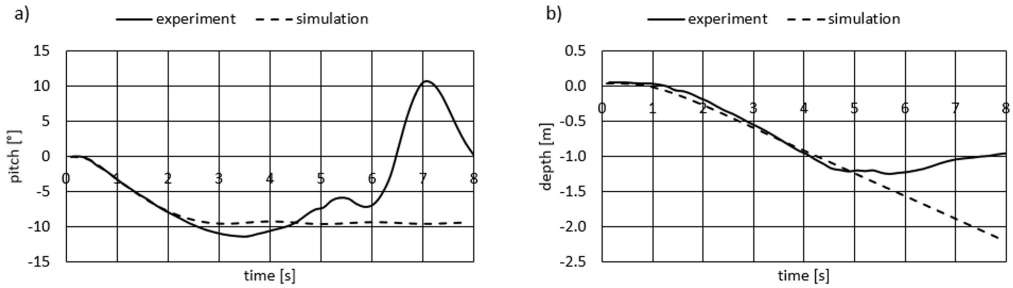

Fig. 19. Pitch angle (a) and depth (b) of the vehicle with fin angle $\delta = 40°$ and velocity $V = 1.15$ m/s.

above the water surface. Although the graphs of the pitch angles slightly differ from each other in the first phase, the depth graphs of Figs. 17(b) and 18(b) show good agreement between the experiment and simulation data. The oscillations of the vehicle body which are visible in the pitch angle do not influence the vehicle velocity vector, which is used to calculate overall depth of the vehicle.

The graphs presented in Fig. 19 reveal slightly different behaviours of the vehicle in the simulation and in the experiment. In the pitch graph presented in Fig. 19 (a) the initial vehicle oscillation does not occur and the experimental data is in good agreement with the simulation. In this test, the thrust force generated by thrusters is large. The fins generate a sufficiently large force so that a slightly positive buoyancy has negligible effect on the pitch angle and the depth for which the experiment and simulations are in good agreement up to the fifth second. The difference in pitch and depth between the experiment and simulation often the fifth second results from the maximal depth of the swimming pool (1.2 m) in which the tests were conducted. In the fifth second, the vehicle hit the floor of the pool causing the pitch angle to change drastically towards positive values. The vehicle also slightly bounced off of the floor and returned to the horizontal position.

The second comparison was made with the results of the second experimental test. The data obtained with the Tracker software are in good agreement with sensors data, so the simulation was performed with the same input signals and compared with the Tracker analysis. The results are presented in Fig. 20. Additionally, Tracker software provides the speed of the vehicle, so the comparison of the simulated and Tracker analysed speed is presented in Fig. 20 (b).

Although the simulation and experimental data in Fig. 20 are not entirely consistent, they fully reflect the character of the vehicle's motion. The depth of the vehicle which is presented in Fig. 20(a) is dependent on the angles α and θ of the vehicle. The smaller pitch angle shown in Fig. 20(b) makes the depth change in the simulation

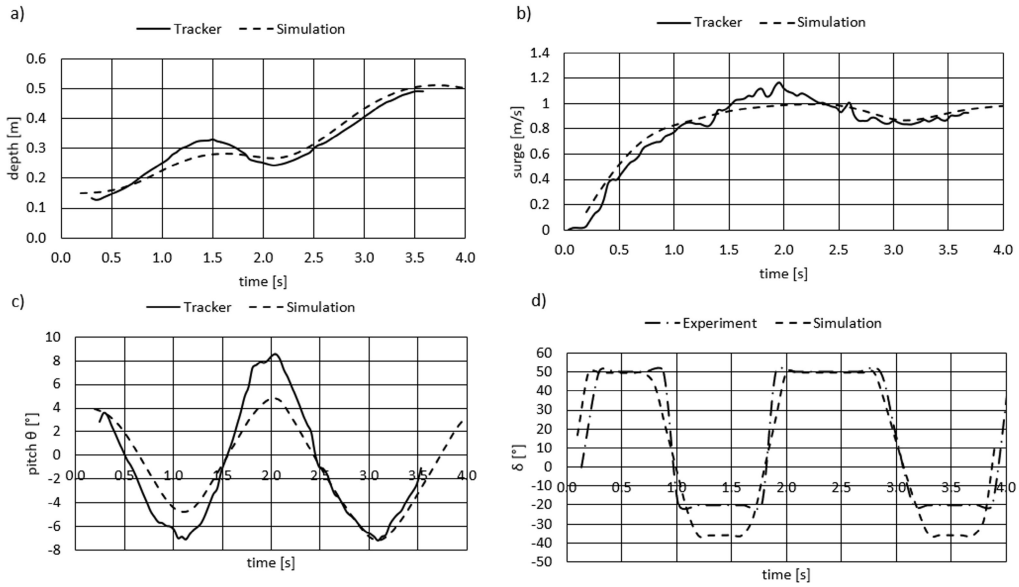

Fig. 20. Comparison of Tracker analysis with simulated data: depth (a), vehicle speed (b), pitch angle (c) and fin deflection (d). .

smaller than that from Tracker. The main reason is the fact that the HUUV had positive buoyancy in the experimental test. At the start of the measurement, 15 cm of the mast was above the water surface. The simulation model assumes neutral buoyancy and full immersion of the vehicle; also, a comparison between the simulation and experiment results was performed to verify whether the model reflects the nature of the vehicle's dynamics. The vehicle motion with the mast above the water surface was not investigated, and this will be done in the future research.

7. Conclusion

In this paper, a simulation model of a vehicle's diving motion was introduced and verified. The HUUV was designed and built at the Faculty of Mechanical Engineering of the Cracow University of Technology. Due to a large mast, the vehicle cannot be considered a streamlined, torpedo-shaped body with three planes of symmetry. To properly design a simulation model, the mathematical model based on Kirchhoff's equations was introduced taking into account the asymmetry in the horizontal plane of the vehicle. Then hydrodynamic coefficients using the CFD SimScale software were estimated, and inertia coefficients were calculated analytically.

To compare the simulation model with experimental data, two different experimental tests were performed. The first test took account of the whole spectrum of available speeds of the vehicle and deflection angles of its fins. The second test relied on parameters measured with sensors placed on board the vehicle and a video analysis of the vehicle's motion in the Tracker software. Then the experimental data were compared with simulated data to verify the diving model. The HUUV diving motion model showed good agreement with the experimental data and its usage is planned in future works to choose proper depth and pitch control strategies of the vehicle. In order to obtain more accurate simulation data, the coupling effects should be investigated between the angle of attack of the vehicle and the angle of deflection of its fins. These effects were neglected in order to provide a linear model of the diving motion.

References

Chae, C. (2021). Depth control of autonomous underwater vehicle using robust tracking control, *Journal of the Korean Society of Mechanical Engineers* **20**(4): 66–72.

Desai, R.P. and Manjarekar, N.S. (2021). Norm-based robust pitch channel control of an autonomous underwater vehicle, *IFAC-PapersOnLine* **54**(16): 258–265.

Fossen, T. (2011). *Handbook of Marine Craft Hydrodynamics and Motion Control*, John Wiley & Sons, Chichester, DOI: 10.1002/9781119994138.

Ha, T., Binugroho, E., Seo, Y. and Choi, J.W. (2008). Sliding mode control for autonomous underwater vehicle under open control platform environment, *2008 SICE Annual Conference, Chofu, Japan*, pp. 1345–1350.

Horak, Tran, T., Nguyen, T. and Hoang, Q. (2020). A motion model of a complex-shaped remotely operated underwater vehicle, *Advances in Military Technology* **15**(2): 343–353.

Huy, T., Choi, H.-S., Nguyen, N.-D., Jo, S.-W. and Kim, J.-Y. (2016). Steering and diving control of a small-sized AUV, *in* V.H. Duy *et al.* (Eds), *AETA 2015: Recent Advances in Electrical Engineering and Related Sciences*, Springer International Publishing, Cham, pp. 619–632.

Jurczyk, K., Piskur, P. and Szymak, P. (2020). Parameters identification of the flexible fin kinematics model using vision and genetic algorithms, *Polish Maritime Research* **27**(2): 39–47.

Kim, K. and Choi, H.S. (2004). Navigation and control for a test bed AUV-SNUUV I, *Proceedings of the 2004 International Symposium on Underwater Technology, Taipei, Taiwan*, pp. 89–94, DOI: 10.1109/UT.2004.1405485.

Ladyżyńska-Kozdraś, E. (2012). Application of the Maggi equations to mathematical modeling of a robotic underwater vehicle as an object with superimposed non-holonomic constraints treated as control laws, *Solid State Phenomena* **180**: 152–159.

Ladyżyńska-Kozdraś, E. (2014a). The dynamic analysis of a torpedo-shaped underwater vehicle as an object with superimposed nonholonomic constraints treated as control laws, *Solid State Phenomena* **210**: 320–325.

Ładyżyńska-Kozdraś, E. (2014b). Robotnic underwater vehicle steered by a gyroscope—Model of navigation and dynamics, *in* T. Březina and R. Jabloński (Eds), *Mechatronics 2013*, Springer International Publishing, Cham, pp. 627–632.

Liu, C., Li, J., Yang, S. and Xiang, X. (2023). Simultaneously tracking and pitch control of underwater towed vehicle with multiple elevators: A finite-time fuzzy approach, *International Journal of Fuzzy Systems* **25**: 264–274, DOI: 10.1007/s40815-022-01270-7.

Maalouf, D., Chemori, A. and Creuze, V. (2015). L_1 adaptive depth and pitch control of an underwater vehicle with real-time experiments, *Ocean Engineering* **98**(2): 66–77.

Malec, M. and Morawski, M. (2014). Analysis of thrust of underwater vehicle with undulating propulsion, *in* R. Szewczyk *et al.* (Eds), *Recent Advances in Automation, Robotics and Measuring Techniques*, Springer, Cham, pp. 453–461, DOI: 10.1007/978-3-319-05353-0_43.

Morawski, M., Malec, M. and Zajac, J. (2014). Development of cyberfish—Polish biomimetic unmanned underwater vehicle BUUV, *Applied Mechanics and Materials* **613**: 76–82.

Morawski, M., Slota, A., Zajac, J., Malec, M. and Krupa, K. (2018). Hardware and low-level control of biomimetic underwater vehicle designed to perform ISR tasks, *Journal of Marine Engineering and Technology* **16**(4): 227–237.

Morawski, M., Talarczyk, T. and Malec, M. (2021). Depth control for biomimetic and hybrid unmanned underwater vehicles, *Technical Transactions* **118**(1), DOI: 10.37705/TechTrans/e2021024.

Petrich, J., Neu, W. and Stilwell, D. (2007). Identification of a simplified AUV pitch axis model for control design: Theory and experiments, *OCEANS 2007, Vancouver, Canada*, pp. 1–7, DOI: 10.1109/OCEANS.2007.4449350.

Petrich, J. and Stilwell, D.J. (2010). Model simplification for AUV pitch-axis control design, *Ocean Engineering* **37**(7): 638–651.

Piskur, P. (2022). Strouhal number measurement for novel biomimetic folding fins using an image processing method, *Journal of Marine Science and Engineering* **10**, Article ID: 484, DOI: 10.3390/jmse10040484.

Piskur, P., Szymak, P., Flis, L. and Sznajder, J. (2020). Analysis of a fin drag force in a biomimetic underwater vehicle, *Nase More* **67**(3): 192–198.

Piskur, P., Szymak, P., Przybylski, M., Naus, K., Jaskolski, K. and Zokowski, M. (2021). Innovative energy-saving propulsion system for low-speed biomimetic underwater vehicles, *Energies* **14**(24), Article ID: 8418, DOI: 10.3390/en14248418.

Sakaki, A. and Kerdabadi, M.S. (2020). Experimental and numerical determination of the hydrodynamic coefficients of an autonomous underwater vehicle, *Zeszyty Naukowe Akademii Morskiej w Szczecinie* **62**(134): 124–135.

Severholt, J. (2017). *Generic 6-DOF Added Mass Formulation for Arbitrary Underwater Vehicles Based on Existing Semi-Empirical Methods*, Master's thesis, Royal Institue of Technology, Stockholm.

Shrivastava, A., Karthikeyan, M. and Rajagopal, P. (2021). Modelling and motion control of an underactuated autonomous underwater vehicle, *2021 6th Asia-Pacific Conference on Intelligent Robot Systems (ACIRS), Tokyo, Japan,* pp. 62–68, DOI: 10.1109/ACIRS52449.2021.9519334.

Steenson, L.V., Phillips, A.B., Turnock, S.R., Furlong, M.E. and Rogers, E. (2012). Effect of measurement noise on the performance of a depth and pitch controller using the model predictive control method, *2012 IEEE/OES Autonomous Underwater Vehicles (AUV), Southampton, UK,* pp. 1–8, DOI: 10.1109/AUV.2012.6380732.

Szymak, P., Piskur, P., Piatek, P., Muchowski, J. and Trawinski, S. (2021). Modeling and simulation of innovative autonomous underwater vehicle past, *2nd International Conference of Maritime Science and Techology, Dubrovnik, Croatia,* pp. 322–346.

Zeng, J., Li, S., Li, Y., Liu, X., Wang, X. and Liu, J. (2017). Research on dynamic modeling and predictive control of portable autonomous underwater vehicle, *OCEANS 2017, Anchorage, USA,* pp. 1–5.

Zhou, H., Liu, K., Li, Y. and Ren, S. (2015). Dynamic sliding mode control based on multi-model switching laws for the depth control of an autonomous underwater vehicle, *International Journal of Advanced Robotic Systems* **12**(7), DOI: 10.5772/61038.

Tomasz Talarczyk was born in 1996. He received his Master's degree in 2021 from the Cracow University of Technology. He presently conducts research towards his PhD in mechanical engineering. His current research activities focus on a swarm of underwater vehicles as well as combining biomimetic and conventional propulsion systems of AUVs.

Appendix

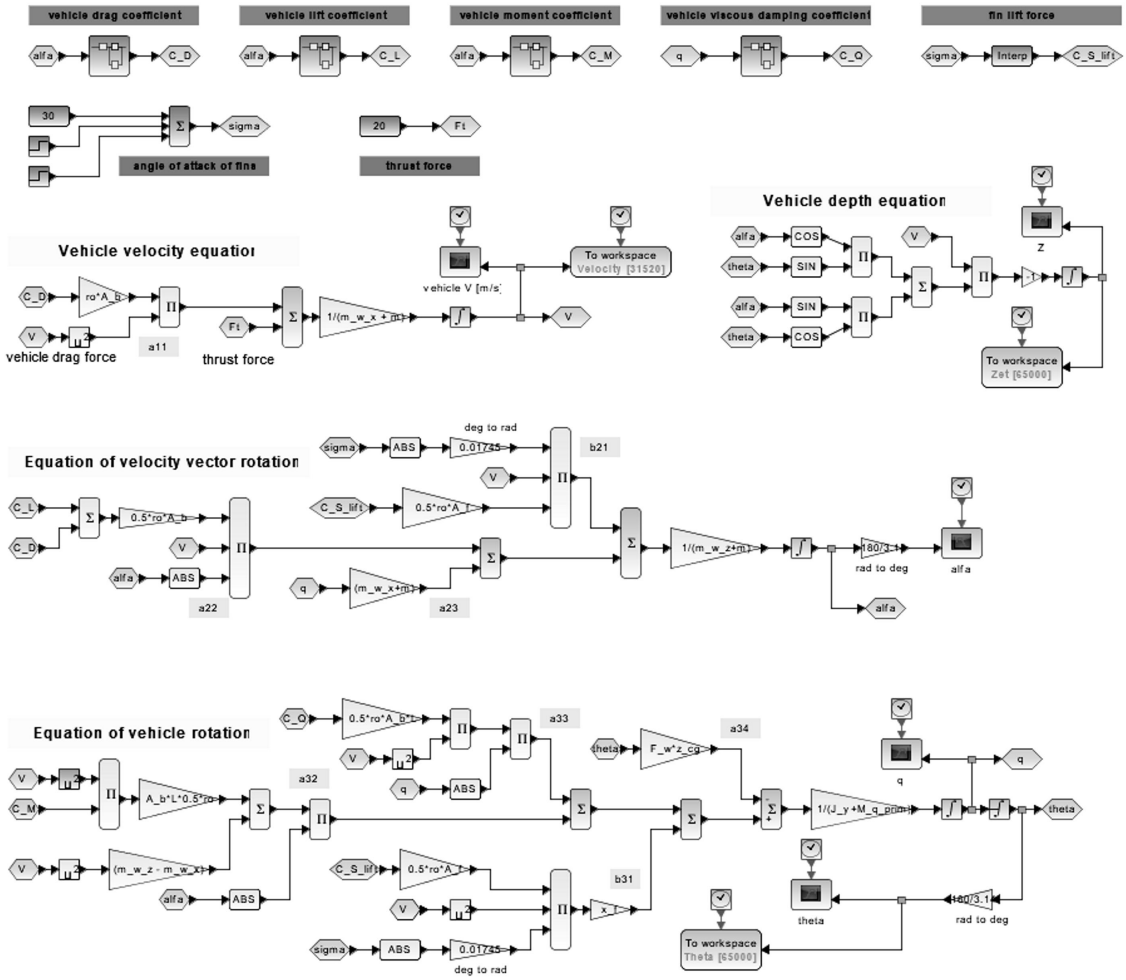

Fig. A1. Simulation model of diving motion implemented in Scilab Xcos.

Received: 2 August 2022
Revised: 4 November 2022
Re-revised: 2 December 2022
Accepted: 1 February 2023